THE 20th CHESAPEAKE SAILING YACHT SYMPOSIUM

ANNAPOLIS, MARYLAND, MARCH 2011

A Multidisciplinary Computational Framework for Sailing Yacht Rig Design & Optimization through Viscous FSI

Vincent G. Chapin
University of Toulouse, ISAE, FRANCE

Nolwenn de Carlan
PHA, Port-Louis, FRANCE

Peter Heppel
PHA, Port-Louis, FRANCE

ABSTRACT

Although competitive sailing yachts may sail fast today this is mainly due to material progress, not sail design. It is always difficult to design a set of sails for a given boat and sailing conditions. A sail has one design shape but an infinite number of corresponding flying shapes depending on materials, trimming, rigging and wind conditions.

In this paper a computational framework for sail analysis, design and optimization has been extended to Fluid-Structure Interaction (FSI) and will be presented.

The multi-physics computational framework is based on a viscous Computational Fluid Dynamics (CFD) solver for the fluid part and on a nonlinear structural modelling for the structural part. A loose coupling of both models has been implemented to be able to make Fluid-Structure Interaction simulations on various sail configurations and to investigate the relation between a design shape and its corresponding flying shapes.

The computational framework presented also contains an optimization package based on derivative-free evolutionary strategies to address complex, non linear optimization problems. It will be used on few examples of sail design questions to illustrate how it may contribute to put some rational elements in a rather frequently passionate discussion between sailors, sail designers, naval architects and amateurs to design the right set of sails for a given boat.

NOTATION

AR	sail aspect ratio (b^2/S)
b	sail spanwise length
β, β_{AW}	apparent wind angle
c	sail chord

$-C_x$, C_r	propulsive force coefficient
C_h	heeling force coefficient
C_m	heeling moment coefficient
C_p	pressure coefficient
δ	sail trim angle
F	effort vector
f	sail camber
f/c	sail camber ratio
Fx, Fr	driving force
h_{CE}	Height of the centre of pressure
I	sail height
J	sail foot in front of the mast
K	stiffness matrix
M	virtual mass matrix
Mx	heeling moment
Overlap	sail foot rear the mast
S	sail surface
V	velocity vector

INTRODUCTION

Fast sailing machines without the gigantism of maxi yachts and without extreme wind (kite surf, wind surf) require a high lift-to-drag ratio as may be seen on the aero-hydrodynamic forces balance on a yacht (Marchaj 1962, Bethwaite 1996, Chapin 2005a). Designing high lift-to-drag ratio sailing yachts is a high-level aerodynamic and hydrodynamic challenge. To face this challenge, two major ingredients are necessary for high speed sailing projects:

- Innovation
- High-fidelity computation

Innovation is needed for radical design evolutions and high-fidelity computation is needed to evaluate the benefit of innovation and to make small changes of the design for best compromise to all round wind conditions.

Studies to increase yacht speed have a long history of wind tunnel tests on sails, towing tank tests on hulls and appendages (Marchaj 1962). Numerical modelling and simulations is a complementary tool largely used today.

Numerous computational models exist. They are based on more or less radical hypothesis. Widely used models for sailing applications involve inviscid equations (potential flow, lifting-line, lifting-surface, vortex-lattice methods) (Milgram 1970, 1971). These models are well-known, computationally efficient, widely used, and well accepted by the sailing community, but the inviscid hypothesis they use is not relevant when flow separation plays a significant role in performance evaluation. And this is not restricted to downwind sailing conditions as is may be seen for example on IACC in upwind conditions in Jones & al. 2001. Separated regions and separation bubbles may be present also in upwind sailing conditions, on real rigs (a mainsail with a mast, a foresail with a stay). As another example, too much camber or too high angle of attack on a gennaker or spinnaker may generate separation on sails. This separation will have a significant impact on lift-to-drag ratio but will not be predicted by inviscid methods. Another example, the mast at the leading-edge of the mainsail generates a separation bubble (Marchaj 1976, Milgram 1978, Wilkinson 1984, 1989, 1990) which will not be predicted by an inviscid solver but will be qualitatively well approximated by a Navier-Stokes solver (V.G. Chapin 2005).

Viscous CFD is a numerical technique initiated in the sixties for laminar flows (Chorin 1967). It has been extended to high Reynolds number turbulent flows in the eighties and widely used in aeronautics. Today, its use begins to be generalized also in nautical studies. This is a numerical model which describes the dynamic of the fluid around bodies based on the resolution of the complete Reynolds Averaged Navier-Stokes equations (RANS), (Chapin & al. 2005, Cowles & al. 2003, Graf & Wolf 2002, Jones & Korpus 2001, Caponnetto & al. 1998). In 1995, Durbin writes that for the first time it is possible to obtain reliable results in three-dimensional viscous flow with separated regions and large separation bubbles (Durbin 1995) as may be present in sail flows. The viscous model increased our understanding of real flow phenomena, and hence opened roads toward better design of complex rigs in an unsteady environment. Moreover, computing time is decreasing each year with increasing computing power (a factor 2 every 18 months). The major drawback of viscous models is probably the high-level of expertise needed to obtain converged, accurate and reliable results for complex three-dimensional flows. Mesh generation, physical modelling hypothesis and numerical choices are some of the few that play a very important role in this process. This implies a second related drawback which is the need for a continuous validation process. Validations through comparisons with wind-tunnel tests and with other numerical simulations are necessary to increase our confidence in numerical results and help the community to define best practices guidelines for high-fidelity RANS simulations. The 4th AIAA CFD Drag workshop held in 2009 may be cited as an example in aeronautics.

Viscous CFD represent a breakthrough for rig aerodynamics study but it is not sufficient because sails are made of soft materials.

For sail design, a second breakthrough is the ability to compute Fluid-Structure Interaction (FSI) of sails through the coupling of a fluid and a structural model. This coupling has begun with inviscid models for the fluid part (Shankaran & al. 2003). Then loose coupling with viscous methods have been developed (Renzsch & al. 2008, 2010, Paton & al. 2008, Trimarchi & al. 2010). The validation process of FSI is a difficult problem. As an example, the relation between flying shapes and rig trim such as backstay tension has been measured on full scale rig with photogrammetry as shown by Augier & al. 2010. But, as said by Hansen 2003, full scale measurements are conducted in an unsteady environment and it is

difficult to measure all relevant data accurately also scatter may be significant.

A third breakthrough will be introduced in this paper with the optimization of three-dimensional sail or rig design and trim through evolution strategies. This new approach to the sail design and trim problem has already been investigated but there are few published results. The principle of the method and some results on an IACC genoa are presented in P. Heppel 2002 with a gradient based optimization algorithm. Shankaran & al. 2003 have shown some interesting results on mainsail-genoa interaction and their consequences on the design with an inviscid fluid model, an adjoint solver and a gradient based optimization algorithm. Chapin & al. 2006 have shown optimization results based on a simplex algorithm and a genetic algorithm for two-dimensional sail and rig configurations.

In the present paper, a computational framework for sail analysis, design and optimization is presented. This computational framework is based on a viscous Computational Fluid Dynamics (CFD) solver based on Navier-Stokes equations for the fluid part and on a nonlinear structural modelling for the structural part. A loose coupling of both models has been implemented to be able to make Fluid-Structure Interaction (FSI) simulations on various sail configurations. The computational framework presented contains also an optimization package based on evolutionary strategies to address complex, non linear optimization problems with a derivative free algorithm. This computational framework will be used on few examples of sail design. The problem of sail design & trim optimization for given wind conditions will be addressed.

Part of the work presented in this paper has been done through a collaboration between Peter Heppel & Associates and “Institut Supérieur de Aéronautique et de l’Espace” (ISAE), during the internship of Nolwenn de Carlan, an ISAE student.

2. FLUID MODEL

In this section, main elements of the computational model are described. Fluid dynamics equations used to simulate the flow around interacting sails are presented with the solver and physical models and limitations. Viscous Navier-Stokes equations on hybrid meshes with structured and unstructured mesh and conformal or non-conformal interfaces between domains have been used. This is a powerful technology which increases flexibility to generate high quality meshes around interacting sails for two and three-dimensional flows.

2.1 Governing equations for fluid

The viscous flow modelling around interacting sails is based on the numerical resolution of the following Reynolds Averaged Navier-Stokes equations:

$$\frac{\partial \rho}{\partial t} + \frac{\partial}{\partial t}(\rho u_i) = 0$$

$$\frac{\partial}{\partial t}(\rho u_i) + \frac{\partial}{\partial x_i}(\rho u_i u_j) = -\frac{\partial p}{\partial x_i} + \frac{\partial}{\partial x_j}[\tau_{ij} + R_{ij}]$$

With the viscous stress tensor

$$\tau_{ij} = 2\mu\,[S_{ij} - \frac{1}{3}\frac{\partial u_k}{\partial x_k}\delta_{ij}]$$

the deformation tensor

$$S_{ij} = \frac{1}{2}(\frac{\partial u_i}{\partial x_j} + \frac{\partial u_j}{\partial x_i})$$

and the turbulent Reynolds stress tensor R_{ij} which should be modelled (see turbulence modelling section). Following Boussinesq hypothesis this tensor may be approximated by:

$$R_{ij} \cong \mu_T\,[S_{ij} - \frac{2}{3}\frac{\partial u_k}{\partial x_k}\delta_{ij}] - \frac{2}{3}(\rho k)\,\delta_{ij}$$

2.2 Solver

Solvers used for the resolution of the Navier-Stokes equations are FLUENT or OpenFOAM.

FLUENT is a steady or unsteady, incompressible, three-dimensional, solver which resolves the previously given Reynolds Averaged Navier-Stokes (RANS) equations. In the present study, the segregated solver and the Spalart-Allmaras turbulence model [Spalart & al. 1992] in its vorticity-based or strain-vorticity-based production term have been used. When not explicitly specified, second-order spatial and temporal schemes were used in its steady version and the importance of that point will be shown in the result section.

The OpenFOAM solver used is a steady incompressible three-dimensional solver with k-omega SST turbulence model and unstructured hexahedral mesh. Accuracy is second order in space and time. The resolution is semi implicit.

To solve the Navier-Stokes equations, proper boundary conditions are required on all boundaries of the flow domain. In FLUENT simulations, at a wall boundary, the no-slip condition is applied. A pressure outlet boundary condition is applied at the outlet. A symmetry boundary condition is used on the top and bottom faces of the domain. A velocity inlet boundary condition is applied on other frontiers (inlet, leeward and windward). In OpenFOAM, at wall boundaries, a no-slip condition is applied, a moving wall is applied on the bottom face, a velocity inlet boundary condition is applied on the inlet and windward boundaries, a pressure outlet condition is applied on the outlet and leeward boundaries and a slip condition is applied on the top boundary.

2.3 Mesh generation

The resolution of the Navier-Stokes equations in RANS formulation is done on unstructured meshes generated by GAMBIT or SnappyHexMesh.

For GAMBIT, unstructured meshes are hybrid non-conformal one with tetrahedral and hexahedral cells (see Figure 1). For SnappyHexMesh unstructured hexahedral meshes are used, with split hexahedral cells at sail boundaries.

On both case, the mesh generation process has been entirely automated. This is an important point of the work which is useful during the FSI coupling and during the optimization process. Because remeshing techniques are used rather than deforming ones, it is possible to have large deformation or design changes during FSI loop or optimization loop.

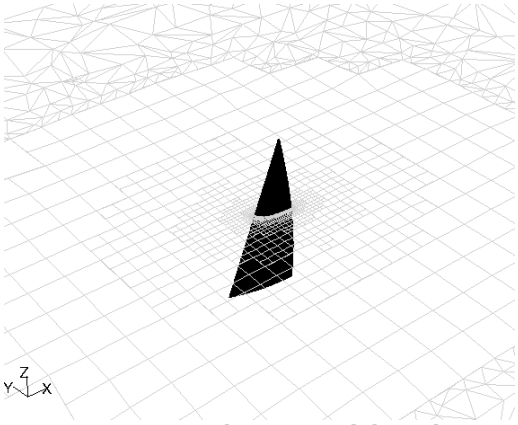

Figure 1: mesh cut around the sail

2.4 Mesh issues

The mesh generation is a crucial step in the process of RANS simulation. It is a time consuming activity which need engineer experience and long practice to rigorously clean the CAD geometry and create the best choice for the mesh topology and generation. The mesh influence on the results of typical sails configurations may be an important issue and should be carefully evaluated and bounded by relevant choices in mesh size and distribution over the flow domain. Boundary layers have to be resolved on bodies (mast and sails) and this imposes some criteria on mesh size in the normal and tangential direction to walls. Flow gradients should be well resolved. This may be a difficult task on typical sails because of the zero thickness and the subsequent leading-edge pressure gradient when angle of attack is not ideal. Based on these constraints, hybrid mesh technology may be a critical issue for high-fidelity RANS simulations [Chapin & al. 2005a].

In fact, results are never totally independent to the chosen mesh. The relevant question when interpreting RANS results on sails is: how bounded is the mesh influence on physical quantities of interest and the required precision. This should be investigated on simplified geometry through validation with wind-tunnel results [Chapin & al. 2005a].

The mesh issues for the prediction of the flow around three-dimensional sails or rigs will be addressed in more details in the results section.

2.4 turbulence modelling

Sail aerodynamic is highly concerned with separation bubble, turbulent transition and turbulent reattachment process and it is well known that these phenomenon and their associated pressure losses may have a critical influence on pressure and friction distribution on sails. Also an accurate representation of laminar and turbulent separated flow regions is critical when we are concerned with drag prediction.

In a previous paper [Chapin & al. 2005b] detail flow analysis with separation regions on mast and mainsail configurations have been computed and for validation purposes. Comparisons were made with wind-tunnel results of Wilkinson [Wilkinson 1984, 1989, 1990]. It has been shown that the Spalart-Allmaras turbulence model may have coherent qualitative behaviour on mast-sail geometries and may reveal to be better than more sophisticated turbulence models based on two transport equations.

The Spalart-Allmaras turbulence model, with standard coefficients values is used on FLUENT. In OpenFOAM, the k-ω SST model is used because of stability problems with the SA model.

3. STRUCTURE MODEL

The structural modelling is based on the software RELAX. It is an interactive, fully non-linear finite-element code to analyse fabric structures using a state of the art relaxation method. RELAX special sail analysis features enables it to predict the behaviour of almost any large-displacement structures. It is a good candidate for sail analysis through a fluid-structure loop.

Implicit or explicit method of resolution can be used to resolve the structural equations. The explicit method is based on Barnes studies [Barnes 1994], using dynamic relaxation and kinematic damping. Dynamic relaxation consists in allocating a virtual mass to each node. Velocity of each node i at time t respect the second law of Newton:

$$\dot{V}_i^t = M_i^{-1} F_i^t$$

With F_i^t the effort vector at t instant

And M_i virtual mass matrix (3*3) of node i

$$M_i = \frac{\Delta t^2}{2} K_i$$

To assure M_i is invertible K_i can be modified using this expression:

$$K_i = f.Id + K_i$$

f value is chosen so that $\frac{EV_{\min}(K_i)}{EV_{\max}(K_i)} \geq k$ where k is a coefficient generally comprise between 0.02 and 0.2 and EV is the eigenvalue. This eliminates very high frequencies which can destabilise the calculation.
Then the acceleration is approached by centred difference:

$$\dot{V}_i^t = \frac{V_i^{t+\frac{\Delta t}{2}} - V_i^{t-\frac{\Delta t}{2}}}{\Delta t}$$

Speed is evaluated at $t + \frac{\Delta t}{2}$ using Euler integration:

$$V_i^{t+\frac{\Delta t}{2}} = V_i^{t-\frac{\Delta t}{2}} + \Delta t . \frac{F_i^t}{M_i^t}$$

And the geometry is updated:

$$x_i^{t+\Delta t} = x_i^t + \Delta t . V_i^{t+\frac{\Delta t}{2}}$$

In the implicit method, the global matrix stiffness K needs to be generated and inverted. If the matrix is singular, springs are added on each node to make the matrix invertible. The stiffness of these springs is adapted for each iteration, it is zero at the end of calculation. The geometry of the model is expressed by:

$$x_i^{t+\Delta t} = K^{-1} F + x_i^t$$

For a N nodes model:

- K is the global stiffness matrix, dimensions N*N
- F is the effort matrix, dimensions N*3
- x is the position matrix, N*3

In both case resolution method is based on a first order time and space discretization.

The model is based on CST (Constant Strain Triangle) membrane elements for sail modelling and beam elements for battens. This model is described like a parametric surface (u,v local coordinates with u and v in [0,1]). Sail materials can be described as a composite material: each ply contains a filament laid or a film. The behaviour of the material can be non linear.

RELAX has a sophisticated meshing tool which can automatically mesh sail geometry given by a CAD software, such as RHINO 3D. Sail meshing is realized using Delaunay triangulation. The grid relates to boundaries of panels and is refined in regions of greatest curvature. During analysis nodes move to their new equilibrium position. There is no remeshing of the structure.

Knowing that a membrane element has no resistance in compression, a wrinkling model is implemented in RELAX to take into account the compressive stresses. As a membrane has an infinite number of kinematics degree of freedom (possibility to deform without a change of stress) and a grid has a finite number of kinematics degrees, the wrinkling modelling allows a better prediction by adding freedom degrees [Heppel 2002].

At that time, the membrane is considered as an orthotropic material with a linear behaviour [Heppel 2002].

RELAX interface presents various possibilities of trimming. This is useful to modify sail shape in a realistic way. In particular, halyard, stay and sheet length can be changed, as well as carriage location In the same way, Relax can reproduce each kind of controls for mainsails (vang, cunningham, outhaul...)

All data are saved from the last analysis. This is a useful point in the case of FSI loop. From a loop to the next one, just the pressure field has to be updated while stresses, geometry and mesh are conserved in memory by the software. This allows for reduced computing time.

4. FLUID STRUCTURE COUPLING

With current computing power and accessibility of specialized software, it is now possible to predict the flying shapes of sails through FSI coupling [Renzsch & al.2008]. The solution at the same time of aerodynamic and structural equations is the best way to achieve this goal but it is computationally expensive [Kamakoti & al. 2004]. A loose coupling method allows a reasonable prediction with a smallest cost by using existing specialized software for the fluid and the structural analysis.

4.1 PRINCIPLE

In a loose coupling method, aerodynamic and structural equations are solved independently. It is possible to use two different programs, one dedicated to structural analysis and the other dedicated to fluid analysis even if they are not developed to communicate with each other. Once for each iteration loop the structural code sends to the fluid code the data concerning the sail shape and the fluid code sends back the pressure field on sail surfaces to the structural code. Iterations are made until convergence is achieved.

4.2 INTERFACING

The aerodynamic and structural solvers are different and don't have the same needs concerning meshing. Their respective meshes are totally independent and an efficient interfacing method needs to be developed to link these modules. In the FSI loop (see diagram 1), the aerodynamic solver sends the pressure field on the geometry to the structural solver and the structural solver communicates the new shape of the geometry resulting from the given pressure field. Also it is necessary to provide a mapping of the pressure field from the fluid mesh to the structural mesh with no prior knowledge of the target mesh.

To achieve this, the coordinate of the structural surface is mapped onto the unit square

using a development of the texture-mapping method described in Desbrun [2002].

When the structural mesh geometry is exported for CFD, we also save a record of the relation between the texture-map coordinates and the current global Cartesian coordinates. We do this by constructing a NURBS surface approximating the structural model with surface parameterization chosen to match the texture coordinates. This provides a good record of the relation between global Cartesian and texture coordinates, although the tensor product NURBS surface cannot capture all the shape details. This NURBS surface is saved in a neutral CAD format.

The CFD typically returns a surface pressure field at global Cartesian positions of the fluid mesh. For each pressure sample point, we associate the pressure value to texture coordinates by finding the closest point on the NURBS surface. This operation is loss-less because every pressure sample is mapped. It introduces position errors of order of the square of the error the NURBS approximation.

Then the new sail shape corresponding to this pressure field is given by the structural solver using an iges file. The new sail shape is used by the aerodynamic mesher to generate a new mesh instead of using a grid moving technique. This choice is more time consuming than moving grid techniques but it is more robust for large displacement membranes and small cells necessary on sail boundary layers for accurate pressure field prediction. The meshing time is about 10% of the calculation time, which seems reasonable.

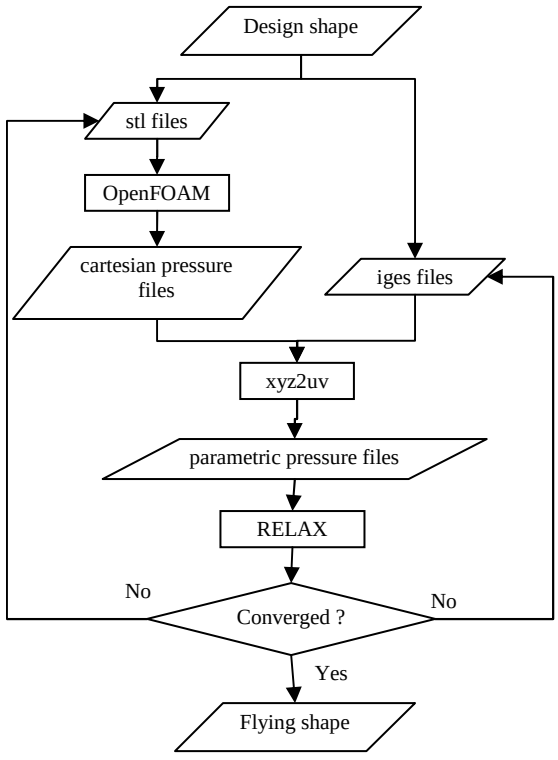

Diagram 1: FSI loop

4.2 LIMITS

This type of loose coupling FSI is not a perfect solution [Kamakoti & al. 2004]. Maintaining accuracy in data exchanges between structural and aerodynamic software is important to obtain relevant aeroelastic results but it is not easy. Stability can also be a problem in particular when aerodynamic stiffness and structural stiffness are of the same order of magnitude. Tests and comparisons are necessary to evaluate different coupling techniques.

5. COMPUTATIONAL FRAMEWORK

Fluid motion around deforming and interacting sails in their real environment is a complex non linear problem. This may be more complex if separated flow, sail configurations with unsteady phenomena related to deformations and wrinkling are considered. Because there are a lot of parameters that define a complete rig design and trimming, there is a crucial need to integrate and automate the entire simulation process in a computational framework. If this is done, it will be easier to understand flow physics and gain insight for better rig design and trim. Turnaround time of the simulation process is a major constraint in common use software. Our computational framework *ADONF* is a response to this problem. It gives us the ability to analyse, design and optimize a large number of rigs configurations. It opens a new way to the design process. It enhances the classical design process, which is based on the designer experience and a trial and error process, by a computational design process able to explore all the interesting regions of the design space through the resolution of an optimization problem.

ADONF integrates and automates the entire computational environment for flow simulation from CAD definition, to mesh generation, flow and structure simulations, flow analysis and design modifications using an optimization loop. This optimization loop is symbolically described on the diagram 2. The main bottleneck of this process is the mesh generation process automation. But it is also a critical advantage over hand made mesh generation as it generates meshes of high reliability and reproducibility. This specific property of automated meshes increases our ability to compare and rank different design or sail trim. It also increases ease to study the mesh density influence on results.

As it will be shown through examples, in the next section, it becomes possible to investigate and resolve new questions about fluid motion around designed bodies and their related performances.

The first level of new questions that can be investigated is the “what-if” questions. What will be the performance of this rig design if I change the mast section? What will be the performance of this rig if I change the sail overlapping factor preserving a constant sail surface? Etc… Only sail designer imagination and time limits the process.

For higher-level questions, biologically inspired optimization algorithms have been implemented in *ADONF* [Rechenberg 1973, Müller 2002, Hansen 2001, 2004]. With optimization algorithms, a second set of questions becomes open for sail researches or sail design. How to change the rig design or the deck plan to increase the performance of that particular sailing boat in given wind conditions? How to change rig trimming to increase boat speed in given wind conditions? What is the best camber and trim of these two interacting sails to maximize driving force or driving to heeling force ratio? This will be illustrated in more details through examples in the results sections.

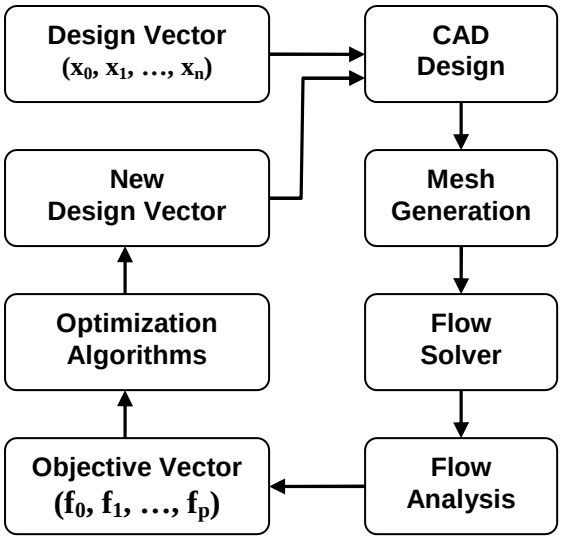

Diagram 2: ***ADONF*** optimization diagram

6. SAIL FLOW PREDICTION & MESH ISSUE

In this work, two different objectives have been chosen for the study of the relevant mesh necessary for a satisfactory flow prediction around three-dimensional sails. The convergence of the relevant physical quantities has been investigated with different mesh resolutions. The first question has been to define the relevant mesh to have nearly converged loads on sails. The second question has been to define the relevant mesh to have qualitatively a right prediction of the main flow features to rank the various design investigated during optimizations.

Figure 2, 4 illustrates the convergence of the driving force with the mesh number of points on a typical full scale sail (18 feet genoa, β_{AW} = 30°, Re = 1.5 x 10^6). Four solutions have been computed on four meshes. Their main properties are resumed in table 1. Meshes are hybrid meshes with a cell size growth rate of 1.2. They are composed of 0.051, 0.18, 0.6 and 2.3 millions tetrahedral cells with hexahedral cells around the sail surface (See figure 1). On this example, the convergence on a critical physical quantity may be observed. Depending on the needed accuracy, the relevant mesh may be chosen. In the following of the paper, 0.18 millions cells has been chosen for optimization problem to reduce computing time and then optimized design obtained has been computed with the 2.3 millions cells mesh to make detailed analysis of the flow.

This configuration has been chosen because it is a difficult one with a separation region on the foot of the leeward side of the genoa. It may be seen on figure 3 that this flow separation is present on meshes M2, M3, M4 but not on the crude one M1. Hence, Mesh M2 has been chosen as a sufficient meshing resolution for ranking during optimization. M1 would probably not because it doesn't detect the flow separation which implies a significant penalty on the aerodynamic performances of this genoa design and trimming.

Table 1 : properties of the meshes

	Volume cells	Sail cells	Wall y+	Fx
M1	51 000	2 650	600	330
M2	180 000	10 800	300	346
M3	600 000	42 500	150	353
M4	2 300 000	170 300	75	355

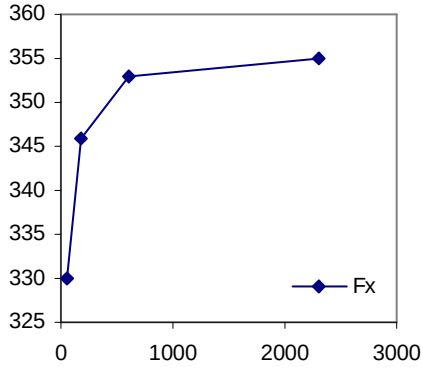

Figure 2: driving force convergence with mesh refinement (number of cells divided by 1000) on GAMBIT mesh and FLUENT solver

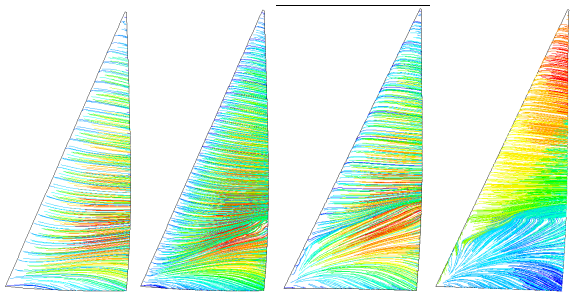

Figure 3 : friction lines on leeward side convergence with mesh: M1, M2, M3, and M4

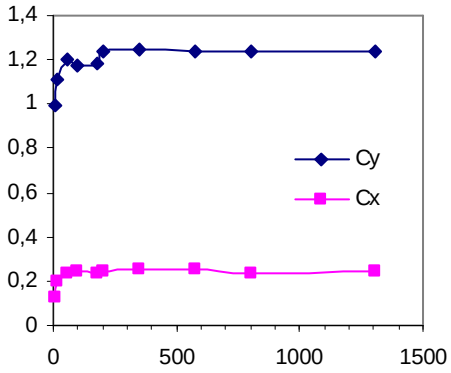

Figure 4 : driving and heeling coefficients convergence (number of cells divided by 1000) with SnappyHexMesh mesh and OpenFOAM solver.

7. AERODYNAMIC OPTIMIZATION OF A THREE-DIMENSIONAL SAIL SHAPE

The first optimization problem consider a mainsail plan form without mast in upwind conditions (V_A=20 knots, β=21°). The optimization problem considered is the following one:

- Objective function : driving force
- Constraint : maximum heeling moment
- Parameters : trim angles and camber values on three sail cuts z/h=0%, 50%, 100%

The optimization begins with an initial sail design and trimming which produce too much heeling moment. The optimization has been done through 491 objective function evaluations through 3D RANS simulations. During the optimization process, various sail flying shapes are selected by the bio-inspired algorithm (CMA-ES) to maximize the driving force with a target heeling moment of 3200 N.m. Some flying shapes selected during the optimization are presented on figure 5 with friction lines on the leeward surface. On the two first flying shapes, it is seen that the flow is clearly not optimized because some separation regions are present on the bottom part of the mainsail. On the two last flying shapes, the flow pattern is optimized. There is no more separation on the leeward side of the mainsail.

Figure 6 shows the convergence of the driving force toward it maximum value with the heeling moment constraint toward the target value (Mx=3200 N.m). This constraint has been implemented by a penalty method (Deb 2001) through the following objective function:

$$f = \left(\sum_{i=1}^{2} f_i \right)$$

Where

$$f_1 = -F_x$$

$$f_2 = \left(\frac{M_x - M_{\max}}{M_{\max}} \right)^2$$

A coefficient and the exponent may be changed to adapt the order of both terms of the objective function to enhance convergence. With the following choice, convergence may be considered as satisfactory after approximately 350 evaluations. This constraint is of high importance for real sail design optimization. Higher convergence rate should be obtained with a higher exponent.

On the following figure 7, the Pareto frontier separates the accessible region of the performance space in the plane (Fx, Mx). This figure shows that the optimization process converged toward a set of solutions that satisfy the heeling moment constraint and maximize the driving force of the sail.

The following table resumes the initial design and trim and the optimized one.

Table 2: results of the optimization

	Initial			Optimized		
z/h	0%	50%	100%	0%	50%	100%
Camber	9%	9%	9%	13%	9%	8%
Trim	12°	12°	12°	12°	15°	22°
Twist	0°	0°	0°	0°	3°	10°
Fx	269			252		
Mx	4074			3203		
Hce	3.82			3.42		

On figure 8 and 9, the last fifty design and trimming are shown to estimates the parameters convergence at the end of the optimization. It is seen that the sail camber of the three sail cuts converge but a significant noise is present. This noise is not equally present on all parameters. It is interesting to note that there is a significant noise on the sail camber at the top from 2% to 10%. The noise is high at the top because the trim angle at the top is nearly the wind apparent angle hence the top doesn't contribute a lot to the driving force. It is the opposite on the middle sail camber. Sail camber is around 12% to 15% at the bottom, 8% to 10% in the middle and 4% to 8% in the top of the sail. In the same way, trim angle of the three sail cuts are around 12% at the bottom, 14% in the middle and 22% in the top of the sail. This results in a global twist of 10°. This twist is not relevant to real twist because it is only the result of the optimization which does not take into account the atmospheric boundary layer in this first version.

It is interesting to note that the optimization does not postulate a positive and monotone twist of the sail but it is found that the best solution to generate high driving force and maintaining a moderate heeling moment is a super linear twist (more twist on top part than on bottom one). The present optimization result is consistent with sail design tendency for highly competitive sails with are based on a super linear twist. This is a rather encouraging result for future optimization.

Examining in more details all the solutions explored during the optimization, it has been found that the two best solutions are of different nature indicating that there are multiple local optimum and probably a global one. The first one is named the

"Optimized" solution in the sense that it results from the convergence of the optimization. The second one is a solution explored at the beginning of the optimization process but is not yet present after the convergence. It is named the "Chance" solution because it has been found by chance when the diversity of the population of solutions was large. These two solutions are of different nature as may be seen in the following table:

	Chance			Optimized		
z/h	0%	50%	100%	0%	50%	100%
Camber	10%	14%	2%	13%	9%	8%
Trim	5°	19°	19°	12°	15°	22°
Twist	0°	14°	14°	0°	3°	10°
Fx	255			252		
Mx	3204			3203		
h_{CE}	3.26			3.42		

The "Optimized" solution uses a lower camber (9% versus 14%) in the middle but a higher angle of attack (6° versus 2°) than the "Chance" solution. These two solutions use two different ways to generate lift (camber or angle of attack). Another difference is the lower altitude of the centre of pressure of the "Chance" solution with a higher heeling force to generate the same heeling moment. This is clearly two different options to design a sail for a given objective as may be seen on figure 10. An interesting point will be to investigate the robustness of both solutions to variations of the apparent wind angle. To do this, FSI will be necessary because for a given design, sail shape will change with the apparent wind angle. Optimization with FSI simulations through viscous CFD and non linear structural calculation has been implemented. Results will be presented in the next section.

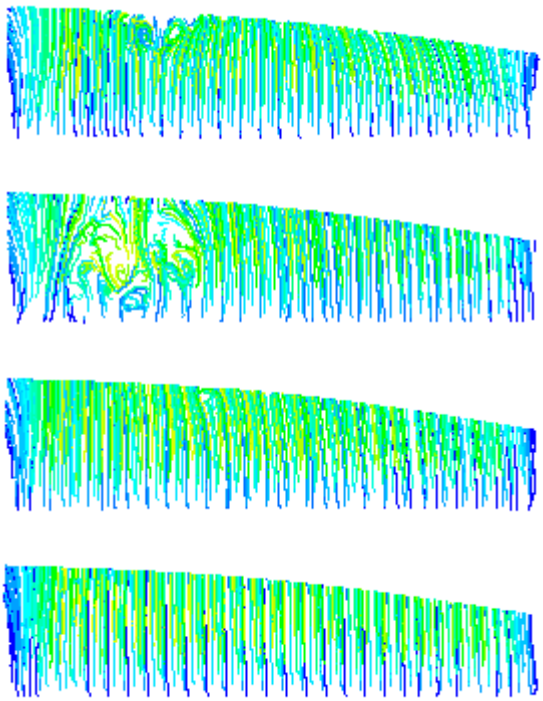

Figure 5 : friction lines on selected sail designs showing convergence toward an optimized design.

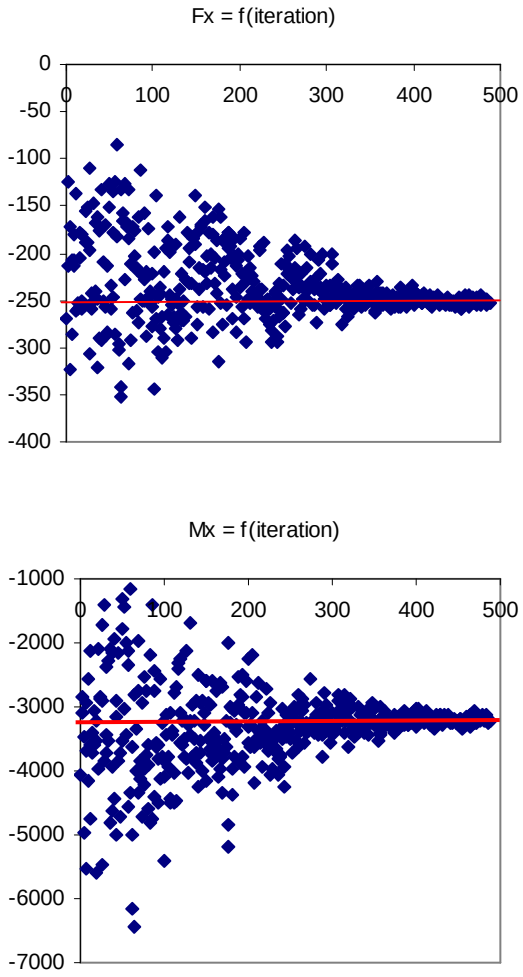

Figure 6 : driving force and heeling moment convergence toward the maximum and the target value during the optimization.

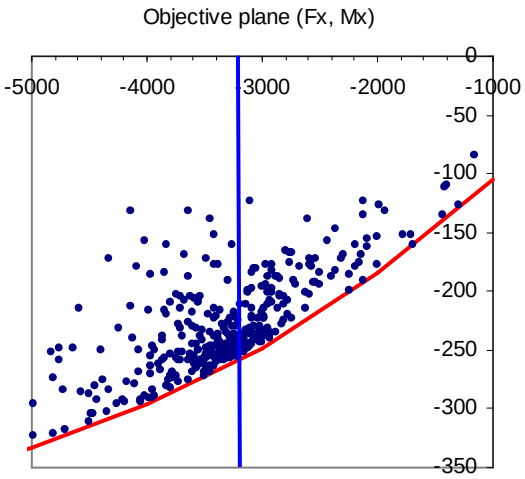

Figure 7 : exploration of the objective space

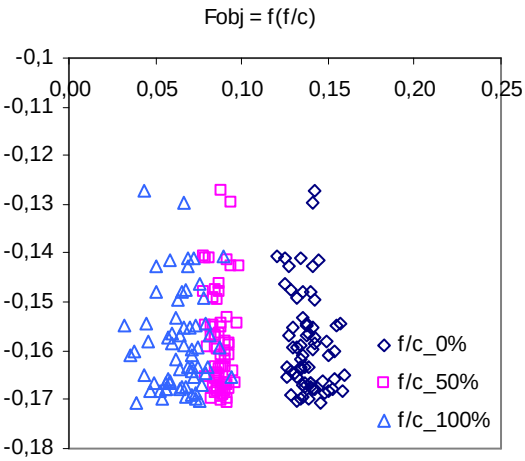

Figure 8 : objective function versus sail camber of the three sail cuts when the heeling moment constraint is satisfied

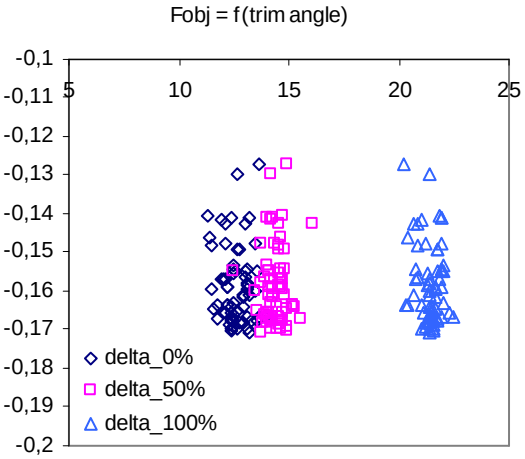

Figure 9 : objective function versus sail trim angle of the three cuts when the heeling moment constraint is satisfied

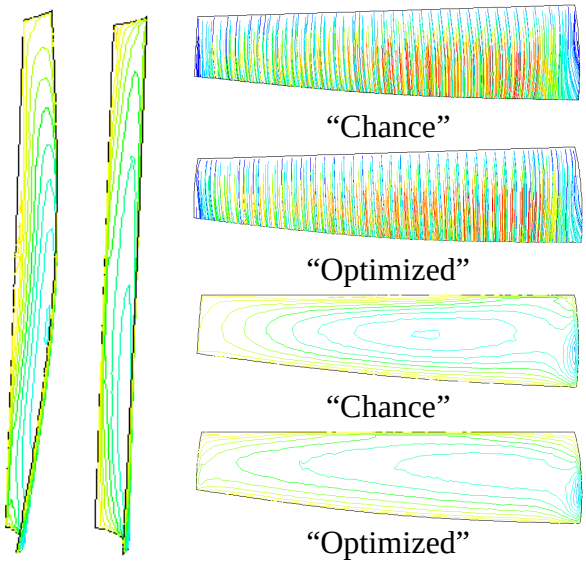

Figure 10 : (left) Chance / Optimized solution with pressure on leeward side (right) friction lines and pressure on leeward side

8. FSI OPTIMIZATION OF A 18 FEET JIB

After implementation and validation of the bio-inspired CMA-ES optimization algorithm through aerodynamic simulations, some results about FSI optimization will be presented in the following part. For aerodynamic analysis meshes used have a cell edge size on the sail surface of order 0.08m which result in a mesh of 150000 cells. For the structural analysis the mesh size is 0.1m.

8.1 Principle

A great feature of the structural solver Relax is to allow easy trimming of every element of the standing or running rigging. Depending on the choice you made for modelling the sail, it is also possible to modify design parameters. Results presented in this section are obtained by changing the value of some parameters controlling the intrinsic shape [Calladine, 1983].

The structure of the sail was chosen to have very little stretch, so that the modification of the flying shape of the sail is a consequence of the intrinsic shape of the sail and the inextensional deformation only. Mean strain in the sail is about 0.2%.

8.2 Optimized jib aspect ratio

For a given jib surface the question is: what is the best plan form of the surface? Is a high but narrow jib better than a larger one with a smaller aspect ratio? The importance of the overlap is also an interesting subject of investigation. With these questions in mind, an FSI optimization problem has been defined and resolved.

A 18 ft rig with a jib interacting with a mainsail is considered. The initial jib design is modified using a two parameters optimization. The parameters chosen for this study, in green on figure 11, are the horizontal distance between the tack and the mast J and the distance between the mast and the clew (overlap). The height of the sail I, in red on figure 11, is imposed by the conservation of the sail surface area. On the boat, the sheet block, the tack point and the hound point (blue points on figure 11), are moving to fit the evolutions of the sail.

The value chosen as objective function is the driving force coefficient Cr, with a constraint on the heeling moment Cm. This constraint is added by using a penalty method.

For the structural analysis the mast is modelled as a rigid object, for the aerodynamic analysis there is no mast.

Results of the FSI optimization are listed in Table 3. It shows the differences of geometry and performances of the initial and the optimized sail design.

Table 3 : geometric characteristics and performances of initial and optimized jib

	J	Overlap	I	Cr=-Cx	Cm
Initial	3.00	-0.10	7.74	0.197	1.14
Optimized	2.60	0.11	8.28	0.202	1.17

The graphs on figure 12 show the driving force coefficient variations of each sail design with the sail aspect ratio AR and the Overlap. The sail aspect ratio has a significant influence on the driving force as expected. A more surprising result is the clear optimum value obtained for the sail aspect ratio AR to maximize the driving force for a given heeling moment constraint. At the opposite, the influence of the overlap parameter on the driving force is not significant on this example. There is a rather smooth optimum with a small overlap of 3% of the jib foot length.

This example shows that for the same sail surface, the shape of the sail can increase or decrease the sail performances. If the jib isn't high enough, as on figure 13a, the flow is detached on a large part of the main sail, just above the hounds point, because the flow is not diverted by the jib. At the opposite, if the jib is too high as on figure 13b, it is very narrow on the top and not able to divert efficiently the flow on the main sail. In the best case found during the optimization, figure 13c, the surface on which the flow is detached is smaller than in both other cases.

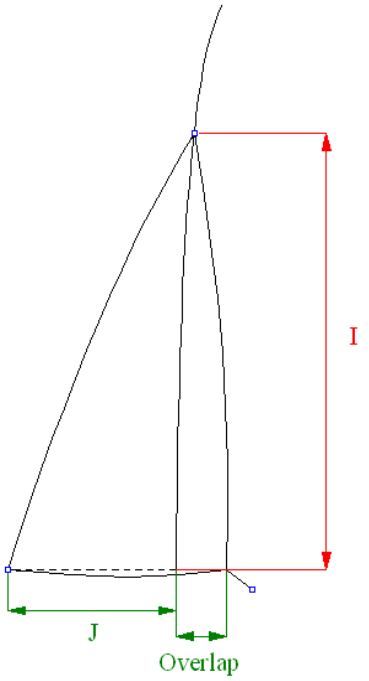

Figure 11 : Optimization parameters

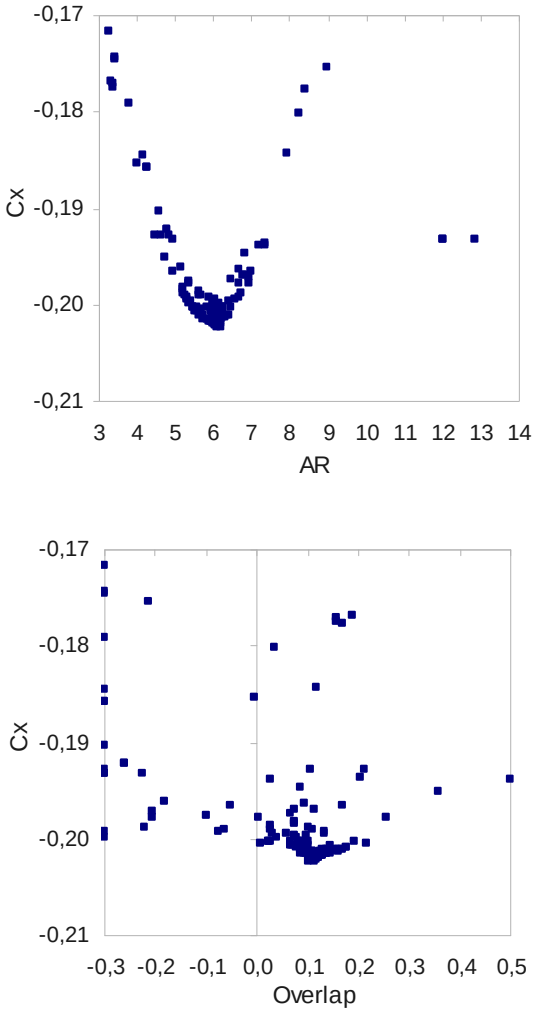

Figure 12 : Design-space exploration

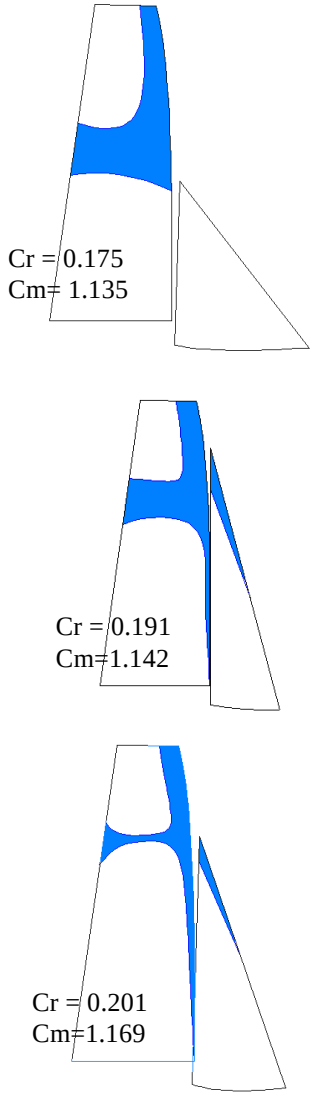

Figure 13 : separated regions on leeward side of the rig for three jibs of different aspect ratio (AR=3.2, 7.9, and 6.1)

8.3 Optimization with a more twisted mainsail

The optimum surface shape of the jib depends of the shape of the mainsail it interacts with. The same FSI optimization as before was made with a different mainsail. Figure 14 shows the two different mainsails. Figure 15 shows the two optimised jibs corresponding to the different mainsails (figure 14). The orange one is designed for the initial mainsail and the blue one for the twisted mainsail. With the twisted mainsail the optimized jib is clearly less high than the previous one. This comparison highlights the role of the jib: it diverts the flow before the mainsail. If the mainsail is very twisted the flow doesn't need to be diverted before the mainsail in order to keep attached. The table 4 describes the dimensions of both jibs and their performances.

More twist on the mainsail has a direct consequence on performance: the driving force and the heeling moment decrease, but figure 16 shows also the displacement of the optimum aspect ratio to a lower value.

Table 4 : dimensions and performances of jibs

	J	Overlap	I	Cr/Cm
Initial mainsail	2.60	0.11	8.28	0.17
Twisted mainsail	3.30	0.09	6.62	0.21

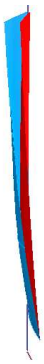

Figure 14: Mainsails used for optimization, in red the first case, in blue the second one. View from aftward

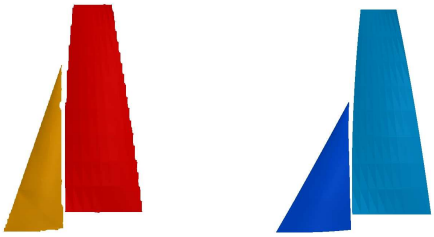

Figure 15 Geometric characteristics of an optimised jib for two different mainsail twist values

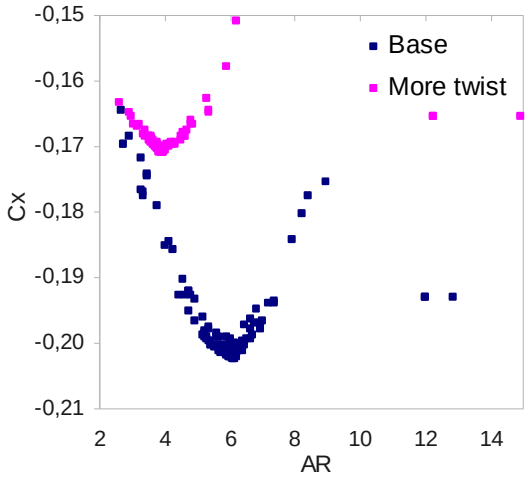

Figure 16 : Cx = -Cr = f(AR)

8.4 Optimization of trimming for each design

A good sail, trimmed poorly, performs no better than a well trimmed sail of a lesser design. So if we want to optimise the design we can't ignore the trimming of the sail. The solution of adding trimming parameters in the optimization process isn't really satisfying. Indeed, each design has its own best trimming and looking for the trimming in the same time as we optimise the design will greatly increase the cost of the optimization.

Another solution is to optimize the trimming for each design, in an intern loop included in the FSI optimization loop of the design. Scheme 3 resumes the principle of the FSI optimization with intern trimming loop.

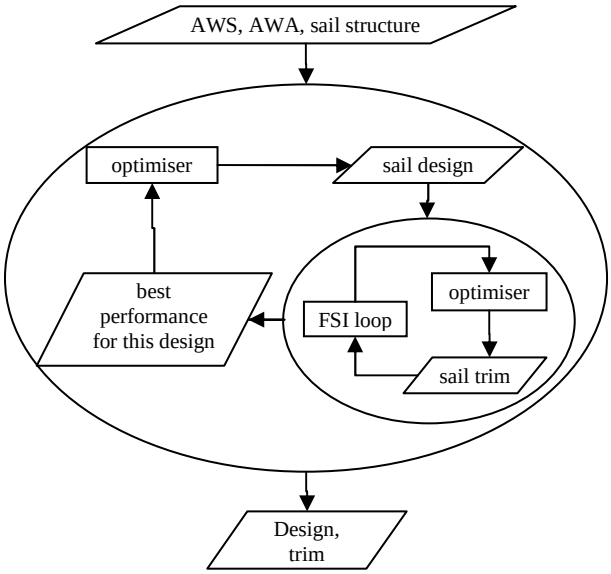

Scheme 3: Double loop optimisation

For each design the best trimming of the sail is found by using the FSI loop presented on scheme 3. Finding exactly the best trimming is not possible; to save time we limit the convergence of the optimization algorithm to 0.005 meter, which means that we are not farther than 0.005 meter from the best trimming. This seems rather good.

Figure 17 illustrates the importance of trimming: a 2 centimetres difference on the sheet length can decrease performances by 1.5%. This is equivalent to change by 8 centimetres the depth of luff curve or to multiply by 3 the broad seams value or to change the aspect ratio by 16%.

As may be seen on following figures and table 5, results with trimming converge toward a different jib design than in the previous part, without trimming.

Figure 18 shows that as the sail gets taller. the sheet length is reduced. The trim used for the previous optimisations was 0.1 meter, because the sail looks nice with this trim but figure 18 shows that this trim was too long for the majority of sails tested.

The main consequence of trimming is to modify the sail twist and then to increase the driving force coefficient of tested designs (figure 19). Higher jib twist lowers its interaction with the mainsail. As illustrated on figure 17, the optimised and trimmed jib has a lower aspect ratio than the jib without trim included. Considering that the non-optimal trim used in the first case was too long, the jib is globally less twisted in this new optimisation. Also, its interaction with mainsail is more important so we don't need such a high jib.

Table 5 : geometric characteristics and performances of the optimised jib with and without trimming

	J	Overlap	I	Sheet	Cr
No trim	2.60	0.11	8.28	0.10	0.202
trim	2.69	0.10	8.04	0.07	0.203

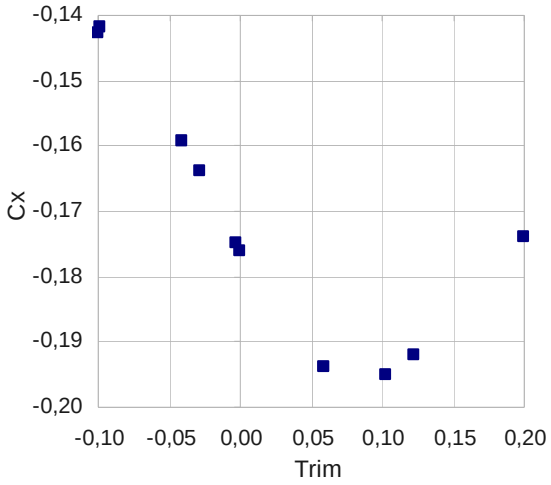

Figure 17 : Cx = -Cr = f (sheet length)

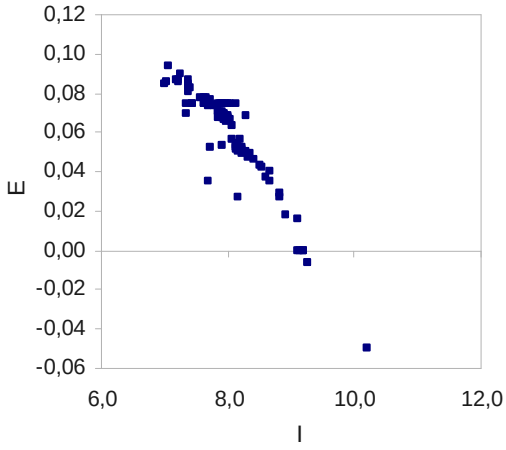

Figure 18 : Best sheet length E versus sail height I

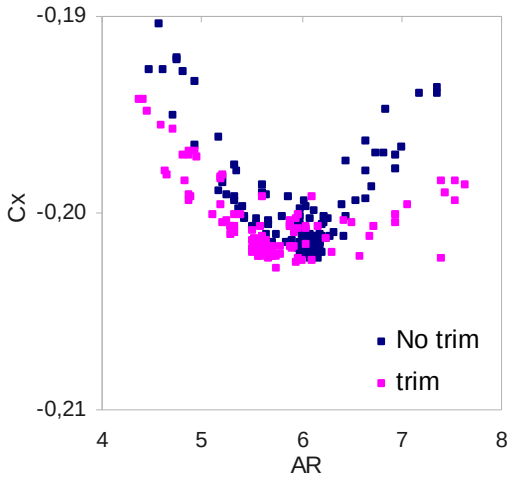

Figure 19 : Cx = -Cr = f(AR) without and with trimming

8.5 Optimized design shape of the jib

The optimization algorithm and the FSI loop allow working directly on the design parameters of the sail. This is interesting in order to design sails which are realizable, and not only theoretical shapes.

Parameters

The parameters chosen for this optimization are the values of broad seams (p1, p2, p3) and the value of luff curve (g), as visible on figure 21. This choice allows optimising the spanwise distribution of Gaussian curvature in a discretised way. Working with broad seams values is an efficient way to reduce the number of optimization parameters; moreover sail makers are familiar with these values. It is possible to realize optimization with other design parameters in order to work with a moulded sail for example.

Performances

As in previous studies, the objective function is the coefficient of driving force, constrained by heeling moment. The table 6 shows the evolution of design parameters and performances after 400 design performances evaluations.

	p1(m)	p2(m)	p3(m)	g(m)	Cr
Initial	0.03	0.02	0.010	0.00	0.194
Optimized	0.040	0.016	0.006	0.096	0.199

Table 6: Geometric characteristics and performances of the initial and the optimised jib

These 4 graphs show the exploration of the objective function when the luff curve and the three broad seams values vary. The optimization algorithm finds a strong design solution for this setting point characterised by a fixed trimming, an apparent wind speed: 21 knots and an apparent wind angle: 21 degrees. The upper broad seam is a parameter more sensitive than the two other broad seams, as illustrated on figure 22. The geometric characteristics of the sail after optimization are listed in table 7:

	25%	50%	75%
entry angle (degrees)	58	59	72
Trim angle (degrees)	12	19	26
camber (% of chord)	16.5	19.7	22.0
camber location (% of chord)	38.9	40.0	44.7

Table 7: Geometric characteristics of the sail after optimization

Compared with a typical jib, the optimised sail has relatively little twist and high camber. The twist of the sail is mainly influenced by the trim, which is fixed in the case considered. The sheet was too tight, so a large camber was needed to keep the flow attached on the leeward side. This is a good illustration of limits of optimisation when the number of parameters is limited by computational cost.

Another remark can be made considering broad seam curve: it is a symmetrical curve, yet a curve giving more volume in the front of the sail is probably better adapted. Indeed, the value of the angle of attack has a great influence on performances, so it is preferable to have the camber which gives the best angle of attack instead of a smaller camber but with a worse angle of attack. Moving forward the maximum position of the broad seam could be a solution to keep the same angle of attack and decrease the camber value.

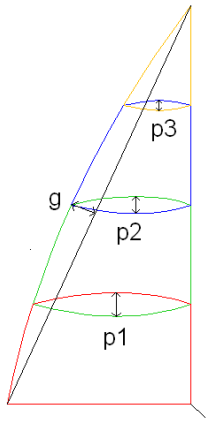

Figure 20 Optimization parameters

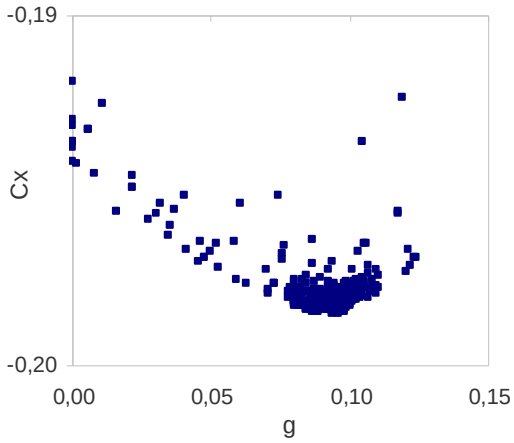

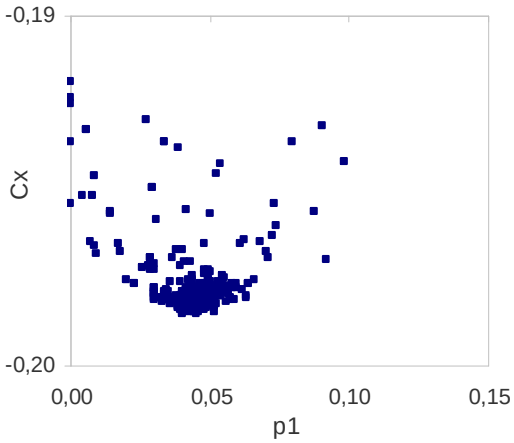

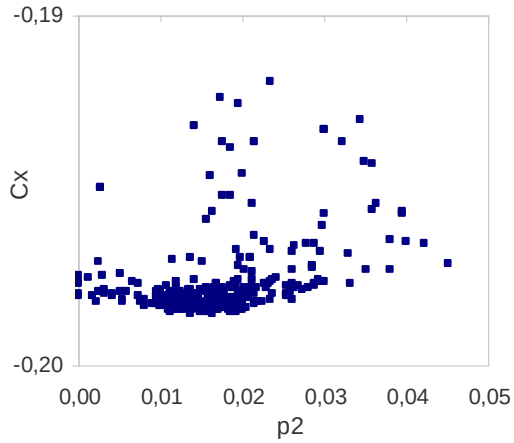

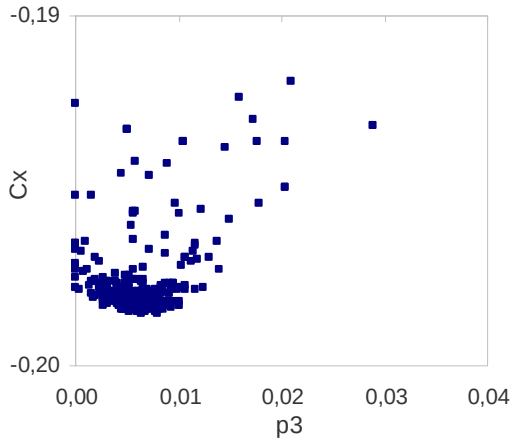

Figure 21 Influence of the design parameters the driving force coefficient Cr = -Cx

CONCLUSIONS

In this paper, a computational framework for sail analysis, design and optimization has been extended to Fluid-Structure Interaction (FSI). This computational framework is based on a viscous Computational Fluid Dynamics (CFD) solver which resolves Reynolds Averaged Navier-Stokes equations for the fluid part and on a nonlinear structural solver for the structural part. A loose coupling has been implemented to make Fluid-Structure Interaction simulations on sails and rig configurations. An optimization package based on a derivative-free evolutionary strategy has been implemented and tested on various three-dimensional sail and rig optimization problems.

The various optimization problems resolved have shown that the evolutionary algorithm chosen (CMA-ES) is a good candidate for aerodynamic and FSI optimization problems. The small size population used and the convergence properties are well adapted for time consuming objective function with local optimum and noisy response.

The heeling moment constraint has been implemented through a penalty method and shows good convergence properties. This constraint plays a central role in sail design and trim.

The aerodynamic optimization of the flying shape of a sail defined by three sail cuts and six parameters and based on the maximization of the driving force for a given heeling moment has converged toward a sail with a super linear twist. This super linear twist is also commonly used by sail designers for the design of highly competitive sails.

The FSI optimizations are preliminary experiments which illustrate the potential of a powerful and robust tool. They also show the dangers of optimization in a limited parameter space. It is essential to include parameters representing crew input. The result is very dependent on the environment, both near and far. For instance, the best shape for the jib depends on the shape of the mainsail. While computing power is limited, great care is

needed choosing the parameters of the optimization and a critical analysis of results is essential.

The present results are exclusively based on aerodynamic performances. But the sails with the best driving force are not necessarily the ones which will make the boat the fastest. The best sail shapes depend as much on the boat's needs. This is place for future work.

ACKNOWLEDGMENTS

Authors wish to acknowledge Mathieu Mellou for his Breizh 18 project which is at the origin of this fruitful collaboration.

REFERENCES

Arden G., "Approximation Properties of Subdivision Surfaces", PhD thesis, University of Washington, Department of Mathematics, 2001.

Augier B, Bot P., Hauville F., Durand M., "Experimental Validation of Unsteady Models for Wind Sails Rigging Fluid Structure Interaction", *INNOVSail2010, Innovation in high performance sailing Yacht*, Lorient, France, May 2010.

Barnes, M., "Form and stress engineering of tension structures". Structural Engineering Review Vol 6 No 3-4 175-202, 1994.

Bethwaite F., "High performance sailing", Waterline Books, p209, 1996.

Calladine C.R., "Theory of shell structures", Cambridge University Press, 1983.

Caponnetto, M. and Castelli, A. "America's Cup Yacht Design using Advanced Numerical Flow Simulations", EPFL Super Computing Review, 10, Nov 1998.

Chapin V.G., S. Jamme and P. Chassaing, "Viscous Computational Fluid Dynamic as a Relevant Decision Making Tool for Mast-Sail Aerodynamics", Marine Technology **42**(1), p1-10, Jan 2005.

Chapin V. G., Neyhousser R., Jamme S. Dulliand G., Chassaing P., "Sailing Yacht Rig Improvements through Viscous CFD", *SNAME 17th Chesapeake Sailing Yacht Symposium*, Annapolis, Maryland, USA, March 2005.

Chapin V. G., Neyhousser R., Dulliand G., Chassaing P., "Analysis, Design and Optimization of Navier-Stokes Flows around Interacting Sails", *MDY06 International Symposium on Yacht Design and Production*, Madrid, Spain, March 2006.

Chapin V. G., Neyhousser R., Dulliand G., Chassaing P., "Design Optimization of Interacting Sails through Viscous CFD", *INNOVSail2008, Innovation in high performance sailing Yacht*, Lorient, France, May 2008.

Chapin V. G., de Carlan N., Heppel P., "Performance Optimization of Interacting Sails through Fluid-Structure Coupling", *INNOVSail2010, Innovation in high performance sailing Yacht*, Lorient, France, May 2010.

Cowles G., Parolini N., Sawley M.L., "Numerical Simulation using RANS-based Tools for America's Cup Design", 16th Chesapeake Sailing Yacht Symposium, Annapolis, Maryland, March 2003.

Deb, K., "An efficient constraint handling method for genetic algorithms", *Computer Methods in Applied Mechanics and Engineering, 186*, 311-338, 2000.

Durbin P., "Separated Flow Computations with the k-ε-v^2 Model", AIAA J. vol 33(4), 1995.

FLUENT 6.1User's Manual, Fluent Inc (2003).

Graf K., Wolf E., "CFD investigations and design integration for IACC yachts", High Performance Yacht Design Conference, Aukland, 4-6 December 2002.

Hansen H., Jackson P., Hochkirch K., "Comparisons of Wind Tunnel and Full-Scale Aerodynamic Sail Force Measurements", IJSCT n°?, 2003.

Hansen, N. and A. Ostermeier (2001). Completely Derandomized Self-Adaptation in Evolution Strategies. *Evolutionary Computation*, 9(2), 2001.

Hansen, N. and S. Kern (2004). Evaluating the CMA Evolution Strategy on Multimodal Test Functions. In *Eighth International Conference on Parallel Problem Solving from Nature PPSN VIII, Proceedings*, pp. 282-291, Berlin: Springer, 2004.

Heppel P., "Accuracy in Sail Simulation: wrinkling and growing fast sails", High Performance Yacht Design Conference, Aukland, 4-6 December 2002.

Jones & Korpus, "International America's Cup Class Yacht Design Using Viscous Flow CFD", 15th Chesapeake Sailing Yacht Symposium, 2001.

Kamakoti, R. and Shyy, W., "Fluid-Structure Interaction for Aeroelastic Applications", *Progress in Aerospace Sciences, 40*, 535-558, 2004

Marchaj, C.A.. "Sailing Theory and Practice". McGraw-Hill, 1962.

Marchaj C.A., "A Critical Review of Methods of Establishing Sail Coefficients and Their Practical Implications in Sailing and in Performance Prediction", 1976.

Milgram J.H., "Section Data for Thin Highly Cambered Airfoils in Incompressible Flows", NASA CR-1767, July 1971.

Milgram J.H., "Sail Force Coefficients for Systematic Rig Variations", September 1971.

Milgram J.H., "Effects of Masts on the Aerodynamics of Sail Sections", Marine Technology, vol. 15(1), 35-42, 1978.

Milgram J.H., Peters D.B., Eckhouse D.N., "Modelling IACC Sail Forces Combining Measurements with CFD", 11th Chesapeake Sailing Yacht Symposium, 1993.

Milgram J.H., “Fluid Mechanics for Sailing Vessels”, Annual Review of Fluid Mechanics, 30, 613-653, 1998.

Müller S.D., “Bio-inspired Optimization Algorithms for Engineering Applications”, PhD Thesis, 2002.

Paton J., Morvan H., Heppel P., “Fluid Structure Interaction of Yacht Sails”, *INNOVSail2008, Innovation in high performance sailing Yacht*, Lorient, France, May 2008.

Rechenberg, I., Evolutionstrategie – Optimierung technischer Systeme nach Prinzipien der Biologischen Evolution, PhD thesis, 1971, reprinted by Fromman-Holzboog in 1973.

Renzsch H., Graf K., “FlexSail – A Fluid Structure-Interaction Program for the Investigation of Spinnakers”, *INNOVSail2008, Innovation in high performance sailing Yacht*, Lorient, France, May 2008.

Renzsch H., Graf K., “Fluid Structure-Interaction Simulations of Spinnakers Getting Closer to Reality”, *INNOVSail2010, Innovation in high performance sailing Yacht*, Lorient, France, May 2010.

Shankaran, S., Jameson, A. and Margot Gerritsen, "Numerical Analysis and Design of Upwind Sails", 21st AIAA Applied Aerodynamics Conference, AIAA Paper AIAA-2003-3498, Orlando, FL, June 23-26, 2003.

Spalart, P.R., Allmaras, S.R., “A one-equation turbulence model for aerodynamic flows”, AIAA paper 92-0439, 1992.

Trimarchi D, Turnock S.R., Taunton J.T., Chapelle D., “Performance The use of Shell Elements to capture sail wrinkles and their influence on aerodynamic loads”, *INNOVSail2010, Innovation in high performance sailing Yacht*, Lorient, France, May 2010.

Wilkinson S., “Partially separated flows around 2D masts and sails”, PhD Thesis, University of Southampton, 1984.

Wilkinson S., “Static Pressure Distributions Over 2D Mast/Sail Geometries”, Marine Technology, vol 26(4), 333-337, 1989.

Wilkinson S., “Boundary Layer Explorations Over a 2D Mast/Sail Geometry”, Marine Technology, vol 27, 250-256, 1990.